



## **TOMOGRAPHIC IMAGING OF CRACK DAMAGE IN CEMENTITIOUS STRUCTURAL COMPONENTS**

Tsung-Chin Hou<sup>1</sup> and Jerome P. Lynch<sup>2</sup>

### **ABSTRACT**

Cement-based materials are widely used in the construction of civil infrastructure systems. However, normal wear-and-tear and extreme loading can result in the damage and deterioration of such important civil structures. In this study, a novel approach to the detection of cracks in fiber reinforced cementitious composites (FRCC) is proposed. The approach is based upon the electrical properties of cementitious materials. Alternating current (AC) signals are introduced in a cementitious component while voltages are measured along the component outer surface. Redundant sets of electrical input-output behavior of a cementitious element can then be used to solve a complex inverse problem in which a multi-dimensional mapping of the internal conductivity of the cementitious material is found. Termed electrical impedance tomography (EIT), the approach has the potential to be used for monitoring the performance and health of cementitious structures in the field. Since cement-based materials are naturally piezoresistive, mapping of the internal conductivity of a structural element would provide an indirect means of mapping internal strain fields. Furthermore, cracks represent a drastic reduction in the conductivity of the component; as a result, conductivity mapping has the potential to also detect and quantify (orientation and dimensions) crack damage. In this study, the EIT approach is formulated and validated upon a set of FRCC structural elements loaded in axial tension. The EIT method proves reliable in identifying localization of crack damage during loading.

Keywords: electrical impedance tomography, damage detection, structural health monitoring

### **INTRODUCTION**

Cementitious materials, including concrete, mortar and fiber reinforced cementitious composites (FRCC), are widely used in the design and construction of large-scale infrastructure systems (*e.g.* bridges, buildings, roadways, dams). While cementitious materials are generally strong in compression, their poor tensile strength results in the formation of crack damage when loaded in tension. To remedy this shortcoming, steel reinforcement is added to concrete to provide the material with tensile strength. Although steel reinforcement enhances the strength of concrete, cracks are still a common occurrence in many concrete structures. Severe cracking is a serious concern if left unattended since cracks can lead to reductions in capacity and can leave buried steel reinforcement vulnerable to corrosion. In recent years, a new class of cementitious composite termed high-performance FRCC (HPFRCC) has been proposed for applications where tensile capacity and ductility are needed. HPFRCC materials consist of small volume fractions of short-fibers (polymeric, steel or carbon) included in a cement matrix. One mechanical attribute that sets HPFRCC apart from traditional FRCC materials is their ability to strain harden under tensile loading; strain hardening

<sup>1</sup> Ph.D. Candidate, Department of Civil and Environmental Engineering, University of Michigan, [tschou@umich.edu](mailto:tschou@umich.edu)

<sup>2</sup> Assistant Professor, Department of Civil and Environmental Engineering, University of Michigan, [jerlynch@umich.edu](mailto:jerlynch@umich.edu)

translates into tensile strength and extreme ductility ( $\varepsilon < 4-8\%$ ) [1]. As a result, HPFRCC has shown the potential for use as a substitute for traditional reinforced concrete in many applications including shear walls and coupling beams [2,3].

While the mechanical properties of cementitious materials have been widely studied, comparatively little research has been conducted in quantifying the electrical properties of cement. The electrical properties of cementitious materials were first systematically investigated in 1955 by Hammond and Robson [4]. Their work largely concentrated upon characterization of the conductivity of concrete as a function of material composition and age. Since their seminal study, many researchers have further characterized the piezoresistive properties (strain-dependent changes in material conductivity) of FRCC and HPFRCC materials [5-9]. The concept of using fibers in a cement matrix to enhance the composite's mechanical properties can be extended to intentionally alter the composite's electrical properties. For example, the inclusion of conductive fibers has shown the potential to increase bulk FRCC conductivities which in turn enhance their piezoresistive properties [8,9].

In this study, a novel approach that utilizes the electrical properties of HPFRCC materials is proposed to detect crack damage. The approach begins by inputting electrical signals (*e.g.* current) and measuring electrical outputs (*e.g.* voltage potential) along the boundaries of a cementitious object. After a redundant set of input-output data is generated, it is used to solve a complex inverse problem whose solution provides a mapping of internal conductivity over two- or three-dimensions. The approach is termed electrical impedance tomography (EIT) and has been carried out in various fields including biomedical engineering and geophysics [10,11]. Development of EIT for FRCC and HPFRCC structural elements will permit the assessment of phenomena closely correlated to conductivity, such as material inhomogeneity, strain, and crack damage. The paper will first present the theoretical formulation of the EIT approach. The approach is then applied to a number of flat plate elements which are constructed from a unique HPFRCC material termed engineered cementitious composite (ECC) [1]. Damage localization that occurs during tensile loading is successfully characterized, including crack location and orientation, using the newly developed EIT method. The paper concludes with a summary of the study findings and a discussion on future research directions for this promising non-destructive evaluation technology.

## **ELECTRICAL PROPERTIES OF FIBER REINFORCED CEMENTITIOUS COMPOSITES**

Fiber reinforced cementitious composites employ short fibers (steel, polymeric or carbon) in a cement matrix to produce a material with tensile properties superior to those of traditional concretes. Within the FRCC material family, HPFRCC materials are a special class that exhibit strain hardening after initial cracking. Through the optimization of the fiber geometry and the fiber-matrix interface, only low volume fractions of fiber ( $V_f < 2\%$ ) are needed to attain strain hardening [12]. When loaded in tension, the strain-hardening behavior of HPFRCC leads to the formation of dense fields of micro-cracks (with crack widths smaller than 100  $\mu\text{m}$ ); this is in contrast to concrete where damage often localizes to form wide cracks. In addition to strain hardening, HPFRCC are ductile and self-confining. As a result, HPFRCC have been proposed for use in earthquake-resistant structures prone to large inelastic deformation and high shear stress demands [2]. Within the HPFRCC material family, various materials have been proposed including engineered cementitious composites (ECC) as reported by Li et al. [1]. ECC, designed at the micro-scale using fracture mechanics, adopts polymer fibers (*e.g.* polyethylene (PE) or polyvinyl alcohol (PVA) fibers) with a surface coating imparting hydrophilic characteristics. No aggregates are included in the cement matrix thereby rendering the material highly homogenous (assuming a uniform distribution of fibers). Composite homogeneity translates into uniform electrical properties throughout the material; this is preferred since electrical homogeneity simplifies the EIT problem and allows one to focus on conductivity changes associated with strain and crack damage.

Cementitious materials, including FRCC, are conductive due to free ions that transport through the matrix microstructure when an electrical potential is applied. The conductivity of the material is a

function of the material composition and environmental factors (*e.g.* temperature, humidity). Cement conductivity often ranges from  $10^{-3}$  to  $10^{-5} \Omega^{-1}\text{cm}^{-1}$ , which is similar to the range of semiconductor materials (*e.g.* silicon). However, the inclusion of conductive fibers can increase the bulk conductivity of the cementitious material by offering paths of lower resistance for the flow of electrical current. The chemical interface between the conductive fiber and the matrix plays an important role in how the inclusion of conductive fibers changes the conductivity of the composite. Researchers have found that the electrical conductivity of the fiber-matrix interface is frequency dependent [7]. During direct current and low frequency alternating current conditions, the fiber-cement interface exhibits high impedance thereby insulating the fiber; the result is an FRCC material whose conductivity is similar to that of the matrix alone. In contrast, when the AC frequency is high, the interface impedance lessens and the composite's electrical properties are strongly influenced by the conductivity of the fibers [7].

Research studies exploring the conductivity properties of FRCC materials have largely focused on their piezoresistive behaviors. Various studies explore changes in the bulk conductivity of FRCC elements as they are monotonically and cyclically loaded in tension and compression [5-9]. Results indicate that in the absence of large aggregates, FRCC materials exhibit linear and repeatable changes in conductivity as a function of strain. The gage factor of FRCC materials have been reported to range from 10 to 60 [5]. Furthermore, the formation of micro-cracking in an HPFRCC is accompanied by a detectable change in the gage factor [8]. While these early results suggest the conductivity properties of FRCC materials can be used for sensing strain and potentially identifying damage, they tend to consider "average" electrical properties measured over large areas and volumes. In contrast to these early works, this study will consider use of EIT to illuminate the spatial variability of the electrical properties of FRCC materials and to map strain fields and damage distributions in two- and three-dimensions.

## ELECTRICAL IMPEDANCE TOMOGRAPHY

Electrical impedance tomography (EIT) is a powerful imaging technique in which a mapping of the internal conductivity of a material can be calculated based upon electrical measurements made along the material boundary. In general, EIT can be broadly divided into three major stages: 1) formulation of the forward problem, 2) input-output electrical data measurements, and 3) solution of the inverse problem.

### Poisson Equation and the Forward Problem

The flow of electricity within a continuous medium can be described by a common differential equation similar to that found in the theoretical description of fluid flow and heat conduction. Provided an electrical input and output to a body ( $\Omega$ ), the electrical potential ( $\phi$ ) along the boundary of the body can be determined by the solution of the Poisson equation (assuming there is no current source or sink on the interior of the body):

$$\nabla \cdot (\sigma \nabla \phi) = 0 \quad (1)$$

The fundamental Poisson equation requires knowledge of the two-dimensional spatial distribution of conductivity  $\sigma(x,y)$  to solve for the electrical potential over the object volume including the body boundary. This is often referred to as the forward problem; given the current applied to the boundary and a known conductivity distribution, the boundary potential  $\phi$  is solved by Eq. 1. In the case of a homogeneous and isotropic conductivity distribution (*i.e.*  $\sigma$  is constant), Eq. 1 can be simplified as Laplace equation:

$$\nabla^2 \phi = 0 \quad (2)$$

In practice, numerical tools such as the finite element method (FEM) must be used to solve the forward problem with a piecewise conductivity distribution within the object. The weak form of the Poisson equation using standard variation methods is formulated by multiplying Eq. 1 by a function,  $v$ , and integrating it over the entire volume [13]:

$$\int v \nabla \cdot (\sigma \nabla \phi) dV = 0 \quad (3)$$

The result is a series of linear equations that describe the electric potential at the nodes of an element given the input/output current applied to the nodes and the conductivity of the element. With a linear set of equations describing the current-potential relationship for an element, the body to be modeled can be meshed into  $M$  elements. Linear equations of the  $M$  elements are then assembled to form a global linear matrix equation that is used to solve the original forward problem,

$$\mathbf{A}\Phi = \mathbf{I} \quad (4)$$

where  $\mathbf{A}$ ,  $\Phi$ , and  $\mathbf{I}$  are the generalized conductivity, potential, and current matrices.

### Electrical Measurements

For a given conductivity distribution and applied currents at the object boundary, the distribution of electrical potential can be numerically determined by Eq. 4. However, the objective of EIT is to determine the distribution of conductivity given applied currents and corresponding potentials measured along the body boundary. The data collection phase of the EIT method begins with the application of electrodes along the boundary of the body. The electrodes are spatially placed at locations corresponding to the nodes of the forward problem finite element mesh. A current generator (Keithly 6221) is adopted to introduce an alternating current in the body by connecting to two adjacent electrodes (one electrode is the source electrode and the other is the sink electrode). This method of current introduction is often termed the adjacent electrode strategy [10]. As the AC current is applied to the element, the electrical potential is measured at all of the other electrodes using a standard laboratory data acquisition system (National Instruments DAQ). Provided the under-determined nature of the inverse problem, a unique solution for the internal conductivity can not be directly determined from Eq. 4. As a result, a high degree of redundancy is needed in the input-output electrical data set to render the problem over-determined and solvable. Furthermore, undesired noise introduced in the electrical measurements due to electrode-surface contact resistance require an even larger set of independent measurements than theoretically needed. As a result, the adjacent electrode method to data collection is applied to multiple adjacent electrode pairs.

### Inverse Problem and Conductivity Reconstruction

Once a FEM model of the forward problem is formulated and a redundant set of electrical input-output data is collected, the inverse problem can be solved. First, an initial conductivity distribution is assumed. The theoretical boundary voltages are calculated by the forward problem (FEM model) assuming the conductivity map and the experimentally applied current. Next, the theoretical voltages predicted by the forward problem are compared to those experimentally obtained. The conductivity map originally assumed is updated and theoretical boundary potentials again calculated. This iterative process is repeated until the theoretical potentials are sufficiently close to those experimentally observed.

The following procedure is adopted to update the initial conductivity distribution so as to force the expected voltage values to converge to the measured ones. The purpose of updating the conductivity map is to minimize the mean square value of the electrical potential difference between expected potential values ( $\phi_{\text{exp}}$ ) and measured values ( $\phi_{\text{mea}}$ ) until it meets a required criterion:

$$\frac{1}{2}(\phi_{\text{exp}} - \phi_{\text{mea}})^T \cdot (\phi_{\text{exp}} - \phi_{\text{mea}}) < h \quad (5)$$

If the mean square error between  $\phi_{\text{exp}}$  and  $\phi_{\text{mea}}$  exceeds the criterion error,  $h$ , the initial conductivity distribution is updated by  $\Delta\sigma$ , which is a function of  $\phi_{\text{exp}}$ ,  $\phi_{\text{mea}}$ , and the directional derivative  $\phi_{\text{exp}}(\sigma)'$ . There are several numerical methods that can be used to obtain  $\phi_{\text{exp}}(\sigma)'$  using the original FEM model. Once the new conductivity distribution is calculated, the forward problem is used again to obtain the expected potential values,  $\phi_{\text{exp}}$ , for comparison to the measured values,  $\phi_{\text{mea}}$ . The procedure is repeated until the mean square error converges to an acceptable value. This approach to reconstruction is also known as Newton-Raphson method and is widely used for solving complex inverse problem such as that posed by EIT.

## EXPERIMENTAL RESULTS AND DISCUSSION

An experimental study is undertaken to validate the use of the EIT method for the detection of cracks in HPFRCC structural elements. In total, six specimens are constructed of ECC: five structural plates (30.5 x 7.6 x 1.3 cm<sup>3</sup>) and one deep beam (140 x 15.2 x 10.2 cm<sup>3</sup>). The fiber type and loading configuration of the six test specimens are summarized in Table 1. While the plates are constructed from various fiber types and volume fractions, the plates are all monotonically loaded in axial tension using a MTS load frame. For each plate specimen, 32 electrodes are placed along their perimeters. Each electrode is made of low resistivity copper tape with silver paste applied between the specimen surface and the copper electrode. Figure 1 illustrates the location of the 32 electrodes installed along a plate perimeter. Furthermore, Figure 2 provides a picture of an actual plate specimen; note the copper electrodes that are affixed to the plate boundary. The adjacent electrode approach to obtaining input-output electrical response data is adopted. Electrical current is applied to each adjacent electrode pair while electrical potentials are recorded at the other electrodes. In this study, the input current is configured to be between 2.4 to 4.7  $\mu\text{A}$  in magnitude and ranging from 70 to 200 kHz in frequency. The actual current magnitude and frequency are adjusted according to the fiber composition of the plate specimen. After the electrodes are installed, an EIT analysis is conducted on each plate numerous times including prior to loading, during strain hardening and immediately following the localization of damage.

Table 1. List of specimens (fiber percentages refer to volume fractions)

Specimen #	1	2	3	4	5	6
Type	Plate	Plate	Plate	Plate	Plate	Beam
Fiber used	1.5% PVA	1.5% PVA	1.5% PVA + 0.1% steel	1.5% PVA + 0.1% steel	1.5% PVA + 0.4% carbon	1.5% PVA
Loading	Tension	Tension	Tension	Tension	Tension	Bending

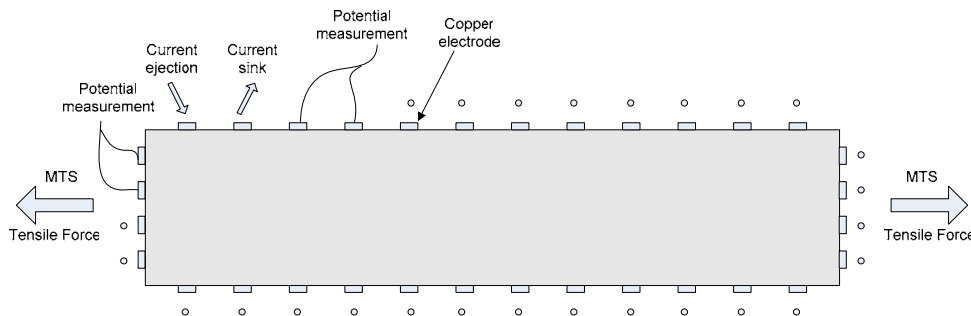


Figure 1. Scheme of electrical impedance tomography (EIT) on ECC plate specimens.

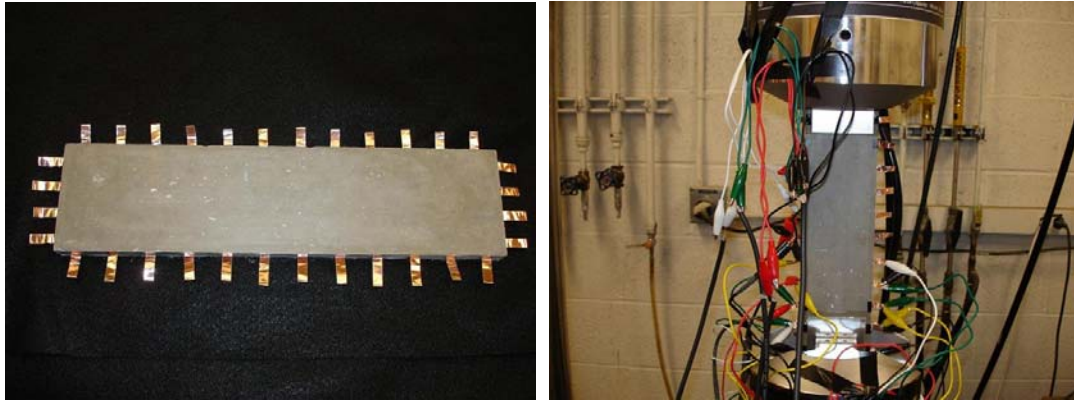


Figure 2. (Left) ECC plate specimen with 32 copper electrodes; (right) ECC plate element loaded in MTS load frame for application of axial tension.

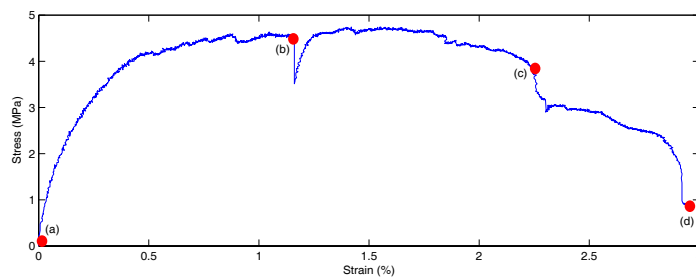


Figure 3. Loading history (stress-strain relationship) of Specimen #1.



Figure 4. Specimen #1 after monotonic loading is completed and damage has localized in the form of two cracks (denoted with red markings to the left and right sides of the plate).

Theoretically, an object with 32 electrodes can produce an electrical image (conductivity map) consisting of 496 elements. However, high contact impedance between the surface of the ECC element and an electrode reduces the resolution of the data collection system (due to a drop in the electrical potential between the object surface and an electrode). To improve the accuracy of the inverse solution, a finite element mesh utilizing a smaller number of elements is pursued; in this study, each ECC plate is meshed using 384 triangular elements. The EIT reconstruction will determine the conductivity associated with each triangular element in the mesh.

Figure 3 provides a plot of the complete loading history (stress-strain relationship) of ECC Specimen #1; Figure 4 presents a picture of the plate after it is removed from the load frame. On the stress-strain plot, four points are noted; each point corresponds to the point where an EIT analysis is conducted on the plate. Point (a) corresponds to the pre-loading state prior to loading the specimen in the MTS machine; point (b) corresponds to the plate undergoing strain hardening; point (c) corresponds to the point when damage localization is visually evident; point (d) is the plate unloaded at the end of the test. At each point, the MTS machine is held fixed to allow the EIT analysis to be conducted. Reconstruction of the ECC plate conductivity, using 384 triangular elements, is presented in Figure 5 at each of the four points along the stress-strain curve. As observed in Figure 5(a), the initial conductivity is fairly uniform with a magnitude of roughly  $300 \mu\Omega^{-1}\text{cm}^{-1}$ . Once the specimen undergoes monotonic tensile loading and strains, the electrical conductivity begins to drop slowly, consistent with the material piezoresistive properties. In Figure 5(b), one can easily see there is a

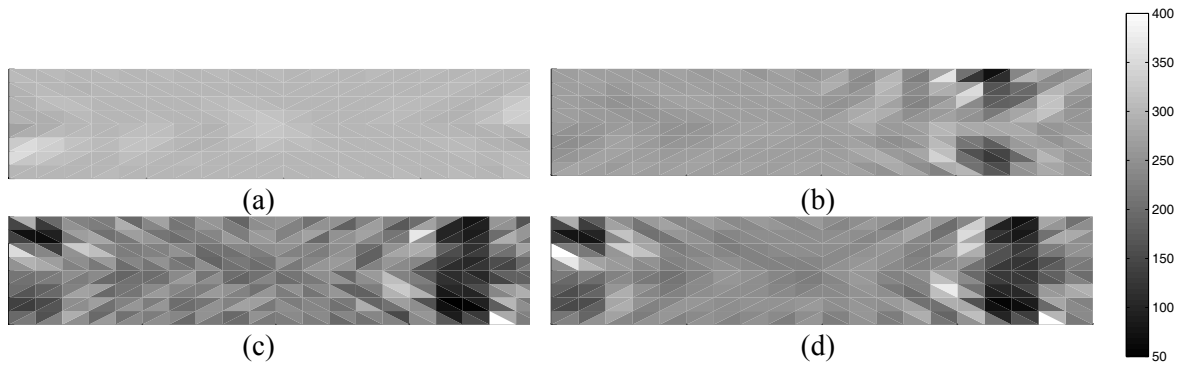


Figure 5. EIT images of plate specimen #1 at each specific state of loading process.

significant change of conductivity near the right hand side of the plate. Although the conductivity is decreasing, no damage is visually evident to the plate except for the formation of some minor micro-cracks. This finding indicates that the EIT is sufficiently accurate to capture the micro-cracking common to HPFRCC materials. As the test progresses, damage localizes to the right side of the plate with a crack propagating through the width of the plate (Figure 4). A thin crack also occurs on the left side of the plate. As shown in Figure 5(c) and (d), the EIT analysis is capable of identifying the formation of the crack on the right hand side of the plate. The electrical conductivity in the vicinity of this major crack was around  $50$  to  $100 \mu\Omega^{-1}\text{cm}^{-1}$ . The EIT analysis is less successful with the crack on the left side although some reduction in the conductivity of the plate is observed to the left of the crack.

Figures 6 through 9 provide the EIT reconstructed conductivities of Specimens 2 through 5, respectively. In general, the initial conductivity of the plate unloaded is largely determined by the type of fiber employed. For example, the plate specimens in which conductive fibers (steel and carbon) are included have higher electrical conductivities. Once the plates were loaded by the tensile loading, the conductivity of each plate drops, especially in locations corresponding to major cracks. The experimental results are consistent across all of the plate specimens tested.

The last specimen to be tested is the ECC beam (Specimen #6). In total, 32 electrodes are placed in a concentrated region of the lower face of the beam where tensile deformation will occur under loading. A 32 cm long region at the center of the beam's lower face is selected for attachment of the electrodes.

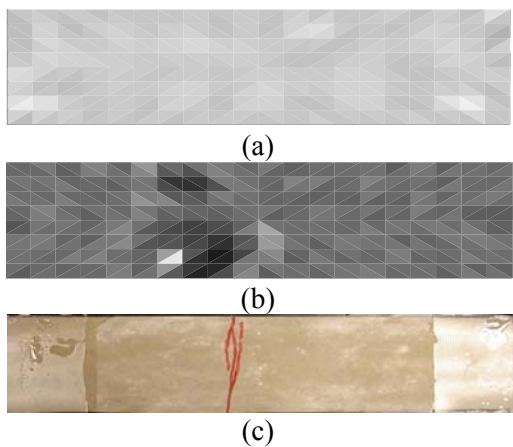


Figure 6. EIT images of Specimen #2: (a) prior to loading, and (b) after damage localization. (c) Damage denoted by red marking.

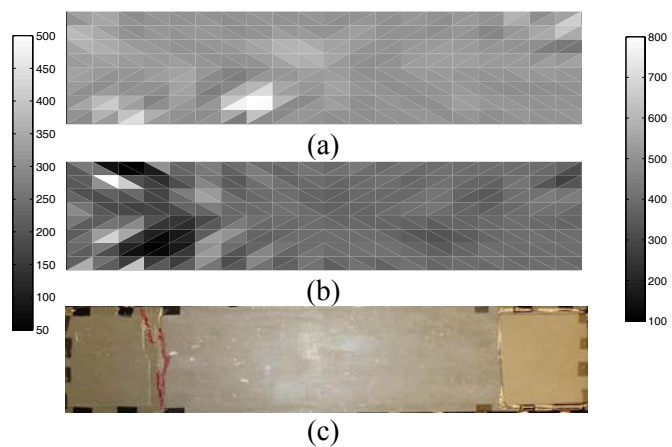


Figure 7. EIT images of Specimen #3: (a) prior to loading, and (b) after damage localization. (c) Damage denoted by red marking.

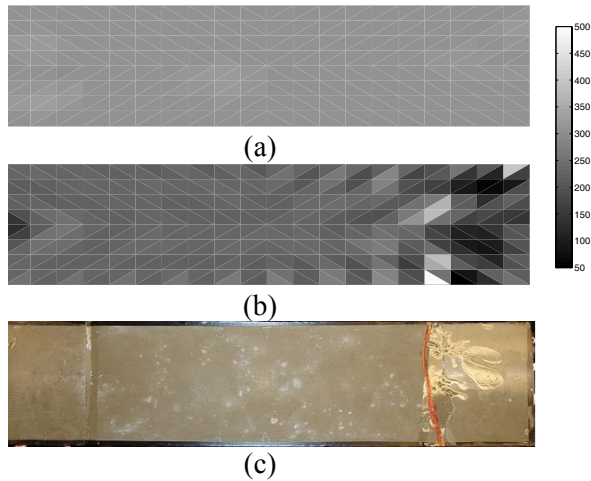


Figure 8. EIT images of Specimen #4: (a) prior to loading, and (b) after damage localization. (c) Damage denoted by red marking.

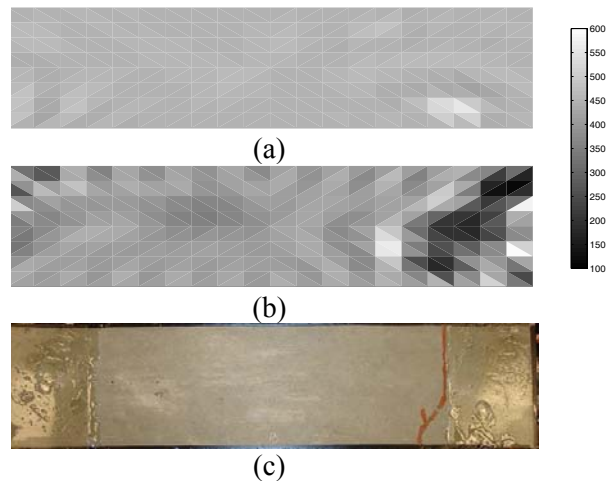


Figure 9. EIT images of Specimen #5: (a) prior to loading, and (b) after damage localization. (c) Damage denoted by red marking.

The beam is then supported by two roller supports spaced 122 cm apart with the electrode region facing down. Applied to the center of the beam's top face is an actuator for 3-point loading. The electrode configuration and a picture of the experimental setup are presented in Figure 10. The beam is loaded with an increasing load while the beam displacement is measured at the center of the span using a high-precision linear voltage differential transducer (LVDT). The final load-displacement curve of the beam is presented in Figure 11. At four points along the load-displacement curve, the test is paused and an EIT reconstruction of the beam's lower face conductivity is made. Prior to loading, at point (a), the conductivity map of the beam is smooth indicating that no defects or inhomogeneities are present along the beam face (Figure 12(a)). After the actuator begins to apply its concentrated load, the conductivity of the beam decreases in response to the tensile strain developing along the bottom beam surface. At point (b) there does appear to be some localization of damage at the center of the beam evident by the lower conductivity (Figure 12(b)); at this point, damage is not yet visually evident. As the beam continues to load, a major crack forms in the center of the beam as predicted by the conductivity map at point (b). At the end of loading, the crack is self-evident with a significant reduction in the conductivity observed at the beam center.

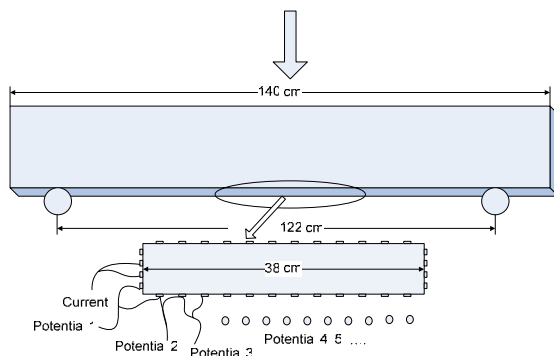


Figure 10. (Left) ECC beam with electrodes applied to lower face. (Right) Experimental setup

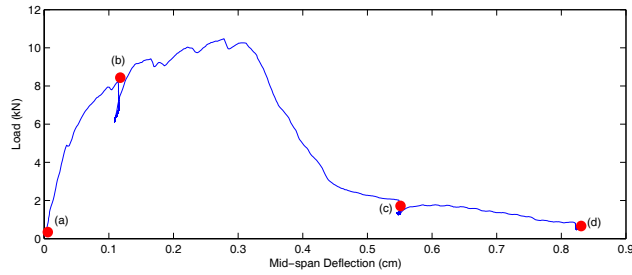


Figure 11. Loading history (stress-strain relationship) of Specimen #6.

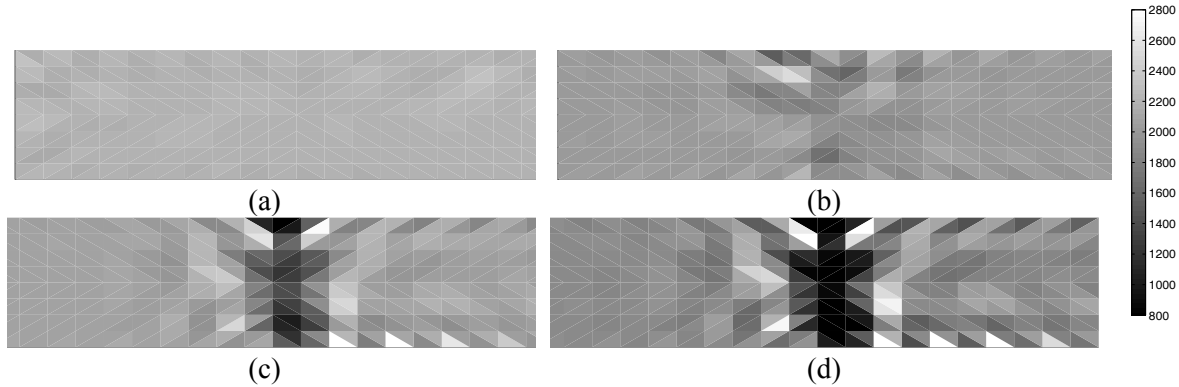


Figure 12. EIT images of Specimen #6 at each specific state of the loading process.



Figure 13. Crack pattern of the ECC beam lower face after damage localization.

## CONCLUSIONS

This study introduces the concept of using electrical impedance tomography to measure both strain and crack damage in HPRCC materials. An inherent advantage of EIT analyses is the mapping of conductivity in multiple dimensions. The addition of conductive fibers to ECC materials enhance their volumetric conductivity and sharpens the observance of crack damage. In addition to detecting wide cracks, the EIT method has shown potential for identifying high strain regions in an ECC element prior to cracking, as well as detecting changes in conductivity associated with micro-cracking. While the results presented in this study are encouraging, further work is needed to improve the method. Future work will concentrate on the development of portable hardware that can be installed in the field; employing wireless sensors capable of electrically querying HPRCC components might resolve issues associated with the complexity of the data acquisition process. Multi-scale methods to the reconstruction process will also be pursued as a means of improving the resolution of the EIT conductivity maps.

## ACKNOWLEDGEMENTS

This research is partially funded by the National Science Foundation under grants CMS-0421180 and CMS-0528867. Additional support was provided by the University of Michigan Horace H. Rackham School of Graduate Studies through the Grant and Fellowship Program. The authors would like to express their gratitude to the National Science Foundation for providing travel support to attend the US-Taiwan Workshop on Smart Structure Technologies held in parallel to the 4<sup>th</sup> International Conference on Earthquake Engineering. In addition, the authors would like to acknowledge the support provided by Prof. Victor Li during the course of this research project.

## REFERENCES

1. Li, V. C., Wang, S., and Wu, C. (2001), "Tensile Strain-Hardening Behavior of Polyvinyl Alcohol Engineered Cementitious Composite (PVA-ECC)," *ACI Material Journal*, v 98, n 6, p 483-492.
2. Parra-Montesinos, G.J. (2005), "High-Performance Fiber Reinforced Cement Composites: A New Alternative for Seismic Design of Structures," *ACI Structural Journal*, v 102, n 3, p 487-495.
3. Canbolat, B.A., Parra-Montesinos, G.J., and Wight, J.K. (2005), "Experimental Study on the Seismic Behavior of High-Performance Fiber Reinforced Cement Composite Coupling Beams," *ACI Structural Journal*, v 102, n 1, p 159-166.
4. Hammond, E. and Robson, T.D. (1955), "Comparison of Electrical Properties of Various Cements and Concretes," *Engineer*, v 199, n 5166, p 114-115.
5. Chung, D.D.L. (2003), *Multifunctional Cement-Based Material*, Marcel Dekker, Brazil.
6. Reza, F., Yamamuro, J.A., Batson, G.B., and Lee, J.S. (2003), "Smart Behavior of Carbon Fiber Cement Composites in Compact Tension," Proceedings of the 16<sup>th</sup> ASCE Engineering Mechanics Conference, Seattle, WA.
7. Peled, A., Torrent, J.M., Mason, T.O., Shah, S.P., and Garboczi, E.J. (2001), "Electrical Impedance Spectra to Monitor Damage during Tensile Loading of Cement Composites," *ACI Material Journal*, v 98, n 4, p313-349.
8. Hou, T. and Lynch, J.P. (2005), "Monitoring Strain in Engineered Cementitious Composites Using Wireless Sensors," Proceedings of the 11<sup>th</sup> International Conference of Fracture ((ICF XI), Turin, Italy.
9. Lynch, J.P. and Hou, T. (2005), "Conductivity-Based Strain and Damage Monitoring of Cementitious Structural Components," SPIE 12<sup>th</sup> Annual International Symposium on Smart Structures and Materials, San Diego, CA.
10. Holder, D.S. (2005), *Electrical Impedance Tomography: Methods History and Applications*, IOP Publishing, Bristol, UK.
11. Zhdanov, M.S. and Keller, G.V. (1994), *The Geoelectrical Methods in Geophysical Exploration*, Elsevier, London, UK.
12. Li, V.C. (1993), "From Micromechanics to Structural Engineering - the Design of Cementitious Composites for Civil Engineering Application," *JSCE Journal of Structural Mechanics and Earthquake Engineering*, v 10, n 2, p 37-48.
13. Vauhkonen, M., 1997. Electrical Impedance Tomography and Prior Information, *Ph.D. Thesis*, University of Kuopio, Finland.